JACS
JOURNAL OF THE AMERICAN CHEMICAL SOCIETY

Article

pubs.acs.org/JACS

Tailoring the Morphology of Mesoporous Titania Thin Films through Biotemplating with Nanocrystalline Cellulose

Alesja Ivanova,[†] Dina Fattakhova-Rohlfing,[†] Bugra Eymer Kayaalp,[†] Jiri Rathouský,[‡] and Thomas Bein[†,*]

[†]Department of Chemistry and Center for NanoScience (CeNS), University of Munich (LMU), Butenandtstrasse 5-13 (E), 81377 Munich, Germany

[‡]J. Heyrovský Institute of Physical Chemistry, Academy of Sciences of the Czech Republic, Dolejskova 3, 18223 Prague 8, Czech Republic

Supporting Information

ABSTRACT: The tunable porosity of titania thin films is a key factor for successful applications in photovoltaics, sensing, and photocatalysis. Here, we report on nanocrystalline cellulose (NCC) as a novel shape-persistent templating agent enabling the straightforward synthesis of mesoporous titania thin films. The obtained structures are highly porous anatase morphologies having well-defined, narrow pore size distributions. By varying the titania-to-template ratio, it is possible to tune the surface area, pore size, pore anisotropy, and dimensions of titania crystallites in the films. Moreover, a post-treatment at high humidity and subsequent slow template removal can be used to achieve pore widening; this treatment is also beneficial for the multilayer deposition of thick films. The resulting homogeneous transparent films can be directly spin- or dip- coated on glass, silicon, and transparent conducting oxide (TCO) substrates. The mesoporous titania films show very high activity in the photocatalytic NO conversion and in the degradation of 4-chlorophenol. Furthermore, the films can be successfully applied as anodes in dye-sensitized solar cells.

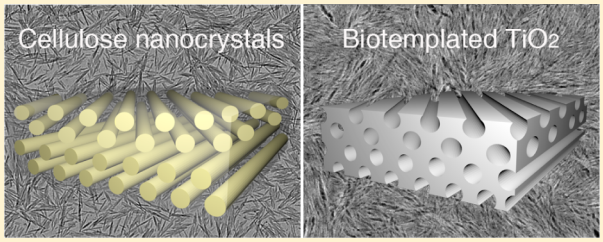

INTRODUCTION

Titania is a very important semiconductor material for photovoltaics, photocatalysis, and electrochemistry. The efficient performance of titania-based devices often requires deposition of porous titania thin films possessing high surface area.[1] Generally, a successful device operation requires not only a high surface area, but also an optimization of the morphology of the titania films, including the crystallinity of the pore walls,[2] as well as the shape, orientation, and size of the pores. Evaporation-induced self-assembly[3] is one of the most popular approaches for the formation of thin films with controlled mesoporosity. The method is based on the self-assembly of titania precursors and structure-directing micelles of amphiphilic molecules.[4] The procedure relies on the formation of micellar aggregates, which is sensitive to the template-to-inorganic precursor ratio, the concentration of amphiphilic molecules, and the nature of the solvents. Considering these factors, the use of shape-persistent templates can be advantageous over molecular template aggregates. As the former templates[5,6] have a defined shape that is maintained throughout the entire synthesis route, it is not influenced by the reaction conditions. Silica and alumina are among the most frequently used hard templates, enabling shape persistent replication of various morphologies. However, removal of the solid inorganic templates without attacking the target material is usually challenging. In this respect, biomaterials are very attractive as shape persistent pore generators since they can provide a wide variety of shapes and sizes and generally they can be easily removed. Several examples of naturally grown biotemplates, such as cell[7,8] and peptide assemblies,[9] egg-white,[10] algae,[11−14] butterfly wings,[15] weevil scales,[16] chitin,[17] and calcium alginate[18] have already demonstrated their potential for the synthesis of diverse porous titania morphologies.

Polysaccharides, in particular celluloses, attract special attention as versatile and abundant "green" templates.[19−22] Natural cellulose, either plant or bacterial, has a hierarchical structure covering a broad range of dimensions. The original fibers of several micrometer thickness can be disintegrated stepwise, first into fibril bundles, then into separate microfibrils and finally into the smallest nanosized crystals composed of cellulose molecules.[23,24] Microbial cellulose has a ribbon-like morphology, with large longitudinal and small lateral dimensions. The plant cellulose fibers, in contrast, are much thicker but the aspect ratios of their crystals are lower than that of bacterial cellulose. The dried nanocrystalline cellulose (NCC) extracted from wood pulp, cotton, and algae has a rod-like shape being 5−70 nm in width and 100 nm to several micrometers in length.[25] The whiskers suspended in water show a remarkable ability to self-organize and to form chiral nematic liquid crystalline phases.[26] Dujardin[27] and Antonietti et al.[28] employed chiral cellulose suspensions in porous silica synthesis. This approach was further developed in the recent studies of Shopsowitz et al. showing a broad variety of NCC

Received: November 11, 2013
Published: February 17, 2014

   dx.doi.org/10.1021/ja411292u | J. Am. Chem. Soc. 2014, 136, 5930−5937

templated chiral materials: colored free-standing silica films,[29] carbon[30] and flexible organosilica.[31] In a recent study,[32] the resulting chiral silica was used as a hard template for the structuring of titania via replication. Direct cellulose templating of titania has been done with nanocellulose aerogels,[33] microfibrillated cellulose,[34] bacterial cellulose,[35] nanocrystalline cellulose,[36] filter paper,[37] and green leaves.[38] However, in all these cases, the final products were sponge-like titania monoliths, free-standing films, or powders. Titania powders biotemplated with cotton fibers[39] and viruses[40] were further processed to a paste that was afterward coated on conducting substrates and applied in solar cell assembly. The direct formation of cellulose-templated titania thin films on substrates has not yet been reported.

Here, we present for the first time the formation of titania porous films on substrates using a direct NCC templating approach. The straightforward one-pot synthesis provides mesoporous TiO_2 thin films with anisotropic porosity deposited on different substrates, which can be used directly as electrodes in photovoltaic devices. The pore anisotropy, surface area, and pore size of the NCC-templated titania can be easily tuned through processing conditions using the same template and without additional swelling agents. The porous morphology can be tailored by the variation of the precursor composition and post-treatment of the film at high humidity. We show a striking effect of the humidity on the templating cellulose crystals. NCC incorporated in the sol matrix swells and expands, which provides a straightforward tool for pore tuning.

Finally, we demonstrate the promising application potential of the cellulose-templated thin films in photovoltaic devices and in photocatalysis, namely in the NO oxidation and 4-chlorophenol degradation in gaseous and liquid phases, respectively.

RESULTS AND DISCUSSION

For the fabrication of the NCC templated titania films, we added an aqueous suspension of nanocrystalline cellulose (NCC) containing rod-shaped cellulose species (Figure S4 of the Supporting Information, SI) to prehydrolyzed titanium(IV) ethoxide (TEOT). After stirring, the opaque colloidal dispersion was coated onto the substrate, and the composite film was calcined at 450 °C to combust the template and to crystallize titania (Scheme 1).

Scheme 1. Synthesis Approach for the NCC-Templated Mesoporous TiO_2 Film

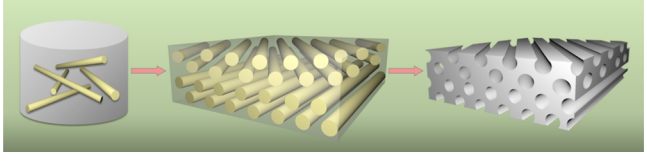

The resulting porous structure (Figure 1b) exhibits slit-shaped mesopores and pore walls consisting of anatase crystallites sized about 9 nm. The pore pattern replicates the parent NCC crystals (Figure 1 and Figure S4 of the SI) that tend to aggregate in short-range bundle-like domains. A similar tendency toward the formation of oriented pore domains is observed in the titania network after template removal. The cross section of the film demonstrates that the domains are

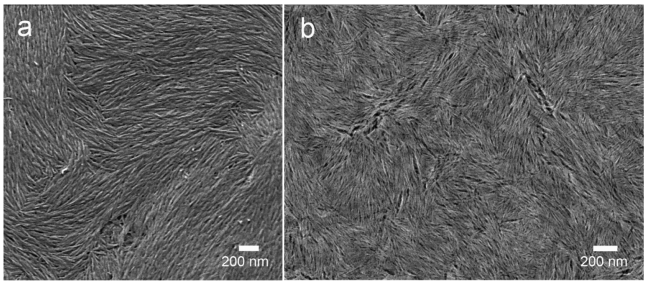

Figure 1. (a) SEM image of nanocrystalline cellulose film prepared by drop-casting a 2.5 wt % NCC aqueous dispersion on a silicon wafer. (b) SEM top view of NCC-templated porous titania thin film spin-coated on a silicon wafer. The precursor solution was prepared by adjusting the TiO_2/NCC mass ratio at 1.5 with 2.5 wt % NCC.

preferentially aligned parallel to the substrate, although some random orientation appears as well (Figure S1a of the SI). The variation of the template distribution in three dimensions enables the formation of a highly interconnected porous network.

We found that the film morphology strongly depends on the titania precursor concentration in the solution. Accordingly, we studied the films coated from different solutions containing the same NCC concentration but different amounts of the TEOT precursor (recalculated as TiO_2/NCC mass ratio, see the Experimental Section). X-ray diffraction (XRD) analysis reveals that the increase in the TiO_2/NCC mass ratio leads to a gradual growth of the average anatase crystallite size after calcination. At the same time, the morphology of the films also changes, as follows from the scanning electron microscopy (SEM) images (Figures 2 and S3 of the SI). Depending on the TiO_2/NCC mass ratio in the precursor solution, one can differentiate three major types of porous structures that are formed after calcination. At the TiO_2/NCC ratio $\leq$0.25, highly porous sponge-like titania is formed that consists of fine 6−7 nm anatase crystallites (region I in the Figure 2). Region II corresponds to the intermediate TiO_2/NCC ratios of about 0.5−1.75. The titania films formed at these ratios feature pronounced pore anisotropy and high pore volume. When the relative TEOT concentration increases further (TiO_2/NCC ratio $\geq$ 2.0), the films become more dense with large slit-like pores surrounded by closely packed large anatase crystallites (range III).

The best results regarding film processability, pore anisotropy, and pore volume were obtained for the TiO_2/NCC ratios of 0.5−1.75, corresponding to the region II. The SEM top-views of these titania films show morphologies that closely resemble the shape of the NCC template. The confined space between the cellulose template crystals restricts the growth of titania crystals in composite materials during calcination. The anatase crystallites are 7−12 nm in size and are homogeneously integrated into the NCC rod pattern. A decrease in the relative NCC amount below this optimum ratio (region III) enables unrestricted growth of the titania crystallites reaching 23 nm after calcination. The NCC templated titania networks show a BET surface area of 61 and 171 m^2/g for the ratios 2.5 and 0.5, respectively. The reason of the marked decrease in the surface area with the increasing TiO_2/NCC weight ratio is the formation of nonporous bulk titania due to the insufficient content of NCC.

In order to investigate in more detail the effect of the NCC concentration on the morphology of the resulting titania films,

dx.doi.org/10.1021/ja411292u | J. Am. Chem. Soc. 2014, 136, 5930−5937

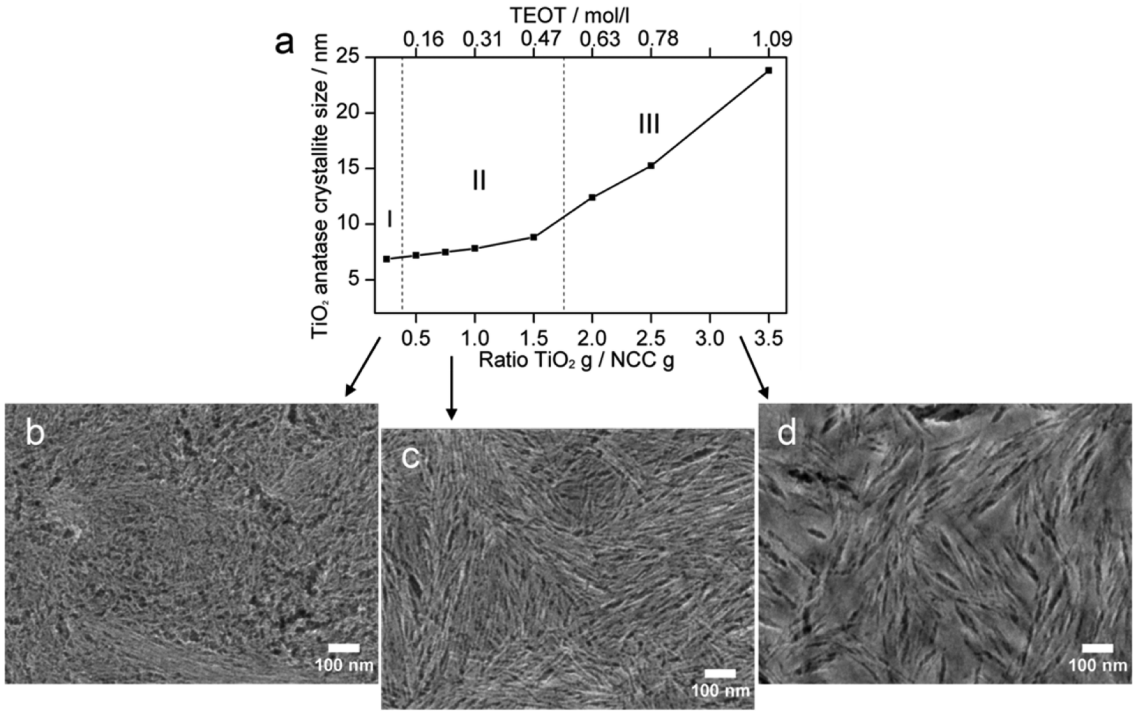

Figure 2. Morphology variation of spin-coated (b-d) and cast (a) NCC-templated titania films depending on TEOT amounts in 25 mg/mL NCC precursor solutions. (a) Development of the mean anatase crystallite size depending on the TiO_2/NCC mass ratio. Scanning electron microscopy top views of porous titania films prepared from the solutions with (b) TiO_2/NCC = 0.25 g/g, (c) 0.75 g/g, and (d) 2.5 g/g corresponding to the regions I, II, and III in the graph (a), respectively.

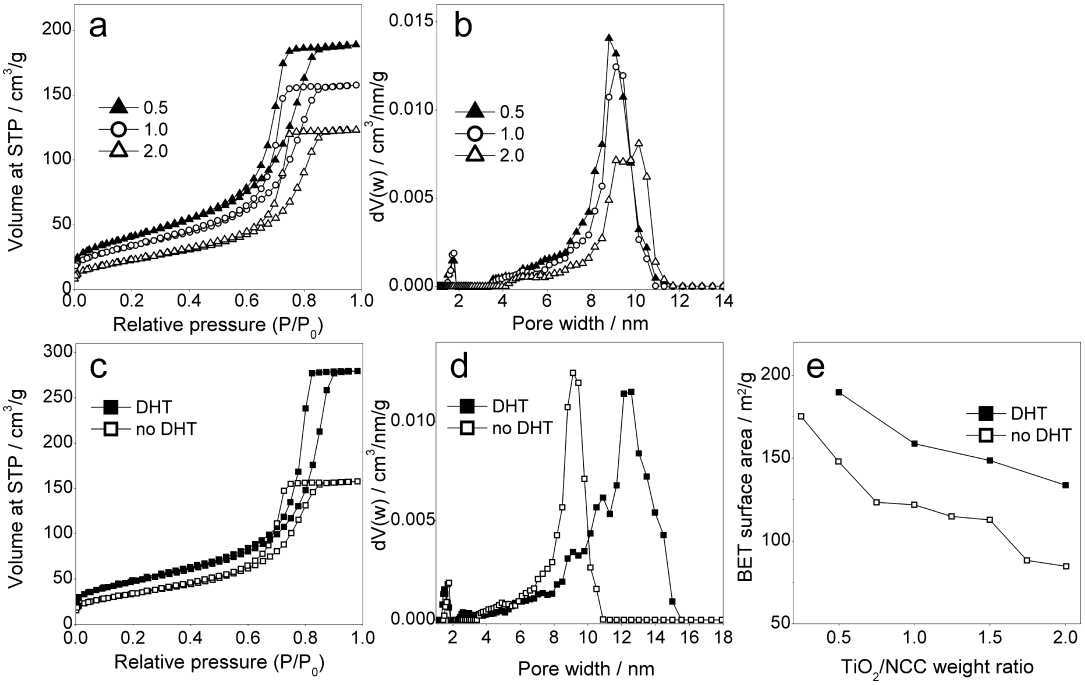

Figure 3. Nitrogen sorption isotherms (a) and corresponding pore size distributions (b) of NCC templated titania prepared from 0.27 mol/L TEOT solutions with TiO_2/NCC g/g ratios of 0.5, 1.0, and 2.0. (c, d, e) Effect of hydrothermal treatment (DHT) applied to NCC/titania-sol composite (TiO_2/NCC = 1.0 g/g) prior to calcination. Nitrogen sorption isotherms (c) and pore size distributions (d) of porous titania after calcination. The sample marked with solid squares (■) was kept for 4 days at 70 °C in 80% relative humidity before calcination and the sample marked with open squares (□) was prepared without the postsynthetic humidity treatment. Variation of the BET surface area of porous titania prepared from precursor solutions with different TiO_2/NCC mass ratios with (solid squares) and without (open squares) DHT treatment (e).

we have kept the TEOT concentration at 0.27 mol/L and prepared solutions with different TiO_2/NCC weight ratios by varying the NCC contents. Nitrogen sorption isotherms of the samples prepared with 0.5−2.0 ratios correspond to the type IV characteristic for mesoporous materials (Figures 3a,c). We found that the surface area and the pore volume of the porous

dx.doi.org/10.1021/ja411292u | J. Am. Chem. Soc. 2014, 136, 5930−5937

titania gradually grow with increasing relative template content (Figures 3e and S11 of the SI). The observed upward trend clearly confirms the suppression of the formation of nonporous material with the increasing percentage of the templating NCC. A related porosity evolution with increasing amount of biogenic template has been observed for chitin-templated porous silica microparticles.[41,42] The templated samples prepared with equal 0.27 mol/L TEOT concentration consisted of titania crystalline domains with dimensions of 7−10 nm (Figures S7 and S8b of the SI).

To elucidate the role of NCC in the structure formation, we have prepared titania from a similar sol−gel titania solution but without NCC. The powders obtained at the otherwise identical conditions are practically nonporous, being composed of densely packed anatase crystalline domains with an average size of 17 nm obtained from XRD line broadening (Figure S8b of the SI). In contrast, titania derived from the NCC-containing solution is highly porous and consists of small (7−10 nm) anatase crystals (TEM images in Figures S1c, S2b, S6, S7 of the SI). NCC fulfills a multiple function in the formation of the porous scaffold and in the crystal growth. The NCC significantly increases the viscosity of the precursor solution. Moreover, NCC rods may also provide an additional surface for the heterogeneous nucleation of titania. We propose that the nucleation of titania on the NCC surface in combination with the confinement effect of the shape-persistent NCC template control the crystallization of the titania scaffold, leading to the formation of polycrystalline scaffolds consisting of extremely small titania crystallites.

As shown above, the variation of the concentration and the relative amount of titania and the NCC template lead to significant changes in the surface area and the crystallite size of the mesoporous titania formed after calcination, but only to a slight change in the pore size distribution (Figure 3b). The pore size is significantly influenced by controlling the NCC degradation during calcination and by applying a humidity treatment to the dried composites prior to their calcination (Figures 3c−e and S10b of the SI). The humidity treatment (usually referred to as delayed humidity treatment (DHT) in the literature) has already been applied successfully for the synthesis of highly ordered tin oxide films[43] and silica.[44] It has been reported that the control over humidity improves the optical quality of films and affects the micelle organization;[45] however, it does not significantly change the dimensions of the resulting pores.[46,47] If pore swelling is of interest when using soft templates, then more significant interventions like addition of swelling agents such as alkylamines or triisopropylbenzene can be necessary.[48,49]

Cellulose has a unique ability to hydrate and swell when exposed to humidity.[50] In addition, cellulose crystals withstand higher temperatures than the majority of amphiphilic molecular templates. Indeed, NCC in the presence of titania precursor and water degrades over a broad temperature range from 120 to 450 °C (Figure S9c of the SI). When the TiO_2/NCC composite is heated, the gradual NCC combustion proceeds simultaneously with the nucleation and growth of the titania crystallites. The control over these two parallel processes is an effective tool for pore size tuning. When a larger pore size is desired, the NCC integrity in the composite should be preserved as long as possible during calcination. At the same time, the titania crystal growth should be slowed down. We found that these requirements can be fulfilled when the dried titania/NCC composite films are additionally treated at higher humidity and at elevated temperatures. Such a procedure can be considered as a hydrothermal treatment of the solid amorphous titania matrix in the confined space of the prearranged NCC template rods. According to our observations, degradation of NCC in hydrothermal conditions is suppressed compared to combustion in dry air (Figure S9 of the SI). This implies that the NCC template is present during nucleation and crystallization of the titania phase, hence constraining the titania crystal growth in favor of smaller crystallites. Additionally, the NCC crystals remain in the swollen state under the hydrothermal conditions, which is advantageous for the formation of the larger pores.

The validity of this concept for enlarging the average pore diameter in the NCC templated titania is confirmed by nitrogen sorption measurements. The data demonstrate an increase in the mean pore size and specific surface area (Figures 3c−e) for the samples treated hydrothermally before calcination. The effect of DHT becomes even more obvious when comparing the total pore volumes of 0.243 cm^3/g and 0.446 cm^3/g for the nontreated and humidity-treated samples, respectively. Despite the pore expansion, the surface area of the porous networks does not drop, but rather increases. It appears that the pores mostly expand while they do not coalesce significantly. Also, the titania crystallites in the hydrothermally modified samples tend to be smaller than in the nontreated samples (Figure S8c of the SI).

The titania films based on the NCC-containing solutions are very smooth, transparent, have a very good adhesion to the substrate and good mechanical stability. Importantly, it is possible to obtain thick (up to about 700 nm) smooth films in a single coating step without adding any thickeners (Figure S1a of the SI). The absence of additional thickening agents assures the smoothness of the films on the nanometer scale (Figure S5 of the SI). The thickness of the NCC-templated titania films can be further increased by successive coating of several layers. The deposition of the following layers does not require any intermediate high temperature calcination, which is often the case for surfactant-templated films.[51,52] For example, for the fabrication of anodes for dye-sensitized solar cells, we have dip-coated four layers. Every subsequent layer was DHT-treated by keeping the films for 1 h in an oven (70 °C/30 min and 100 °C/30 min) in a desiccator with a saturated KCl solution. During the hydrothermal treatment the titania scaffold already starts to crystallize. At the same time, the NCC does not dry out such that the film volume remains preserved. After the intermediate humidity treatment, the partially crystalline titania films sustained the final calcination at 500 °C/30 min and turned into a highly porous titania network. It is possible to tune the final film thickness by controlling the drying conditions of each deposited layer, as well as by adjusting the NCC concentration in the precursor solution (not shown).

We note that the deposition protocol for the mesoporous films based on the NCC containing solutions is much more straightforward and less time-consuming than in the case of films templated by more traditional molecular surfactants. For example, the thickness of the titania films obtained by a sol−gel route from the solutions containing amphiphilic polymers is usually limited to about 300 nm. The main reason for this limitation is a drastic change in volume upon combustion of the polymer and crystallization of an initially amorphous mesostructured framework upon calcination, leading to cracking and even peeling off the substrate for the thicker titania coatings.

dx.doi.org/10.1021/ja411292u | J. Am. Chem. Soc. 2014, 136, 5930−5937

Mesoporous titania is important from the environmental point of view, as it can be used for the photocatalytic degradation of a number of pollutants. In the following, we present two examples of the photocatalytic performance of the NCC-templated titania, namely in the oxidation of nitrogen oxide and in the degradation of 4-chlorophenol in aqueous media, serving as models for the purification of air and water, respectively. To assess the efficiency of the NCC-templated titania as a photocatalyst, its performance was compared with recently published data on mesoporous layers of TiO_2.

For the photocatalytic experiments the film was spin-coated on a glass substrate from a precursor solution with a TiO_2/NCC weight ratio of 0.75 and calcined at 500 °C. The film shows excellent transparency (Figure 4b) and high porosity

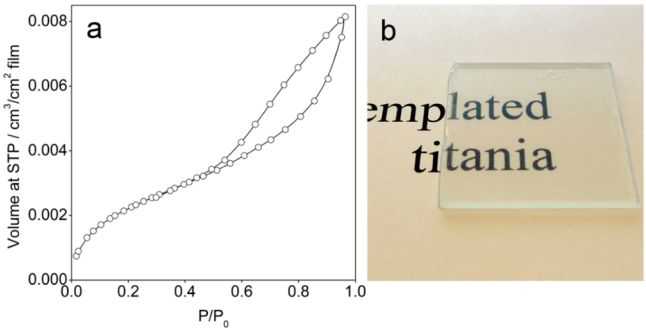

Figure 4. Transparent NCC templated titania porous film of 850 nm in thickness coated on a 2.5 × 2.5 cm^2 glass substrate; (a) adsorption isotherm of Kr at 77 K and (b) a photo.

according to the sorption measurements. The adsorption isotherm of Kr at the boiling point of liquid nitrogen (ca. 77 K) exhibits a broad hysteresis loop ranging from the relative pressure of ca. 0.5 to 1 (Figure 4a), which indicates the presence of some proportion of mesopores narrower than ca. 10 nm. As the adsorption isotherm does not reach a plateau at a relative pressure approaching 1 and keeps rising, the film must additionally contain a substantial proportion of pores wider than about 10 nm. This conclusion follows from the peculiar properties of krypton in narrow pores at ca. 77 K, which behaves as a supercooled liquid. The specific surface area of the film derived from Kr sorption measurements and related to substrate area, film total volume or film mass equals 112 cm^2/cm^2, 132 cm^2/cm^3, and 115 ± 8 m^2/g, respectively. The estimated film porosity is 68% as calculated from the total volume of the film, its mass and anatase density. Using the pore volume calculated from the adsorption isotherm of Kr, the fraction of pores narrower than about 10 nm is 17%. The nitrogen sorption data of the free-standing film prepared from the same precursor solution showed a BET surface area of 123 m^2/g. The similarity of the BET surface area of the powder determined by N_2 adsorption and that measured on the thin film by Kr sorption shows (i) that the films are homogeneous and (ii) that their porosity does not significantly change with the thickness and the deposition method.

Owing to the high porosity, high crystallinity and anatase phase present, the NCC-templated porous titania films deliver a high steady-state conversion efficiency of 16% in the photocatalytic oxidation of NO. Its performance compares favorably with that of the "brick and mortar" mesoporous films templated by amphiphilic Pluronic polymer, which at the same conditions achieved a conversion of 10%.[2]

The reaction mechanism of the photocatalytic degradation of 4-chlorophenol is complicated but the overall decrease in the concentration of 4-chlorophenol can be described by a first-order reaction[53] (Figure S12 of the SI). The calculated first order rate constant for the photocatalytic decomposition of 4-chlorophenol on the NCC-templated titania film equals 0.18 h^{-1}, which is 50% higher than the highest reported rate constant of 0.12 h^{-1} obtained at exactly the same conditions (especially the intensity of illumination and the illuminated area were identical) for a 1.5 μm thick mesoporous sol–gel titania film with 456 cm^2/cm^2 roughness factor, prepared using Pluronic P123 block-copolymer.[53]

In addition to their high photocatalytic activity, the NCC-templated mesoporous titania films show excellent performance as thin anodes in dye-sensitized solar cells (DSSCs) (Table 1

Table 1. Photovoltaic Parameters of the Dye-Sensitized Solar Cells Made with Different Titania Anodes, N719 dye and I^-/I_3^- Electrolyte[a]

titania anode	film thickness (μm)	J_{sc} (mA/cm²)	V_{oc} (mV)	*FF* (%)	η (%)
(a) NCC-templated	1.8	6.02	731	70.9	3.12
(b) Sintered NPs	2.5	5.24	715	72.2	2.70

[a]The cells were measured under AM 1.5 G at 100 mW/cm^2 full sun irradiation.

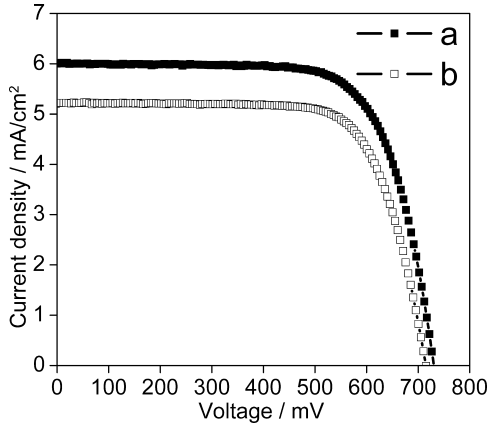

Figure 5. I–V curves of DSSCs prepared with (a) 1.8 μm NCC-templated mesoporous titania film acting as an active electrode (solid squares) compared to the performance of (b) a 2.5 μm thick anode made of sintered 20 nm titania nanoparticles (open squares). The anodes were sensitized with N719 dye and assembled in a sandwich-type cell with volatile I^-/I_3^- electrolyte and Pt-counter electrode. The photovoltaic performance was measured at AM 1.5 G at 100 mW/cm^2 full sunlight illumination. The active cell area was 0.159 cm^2.

and Figure 5). A film of only 1.8 μm thickness obtained by the subsequent coating of 4 layers (see Experimental Section for detailed description of the synthesis) delivers a short circuit current density l_{sc} of 6.02 mA/cm^2 at full sunlight (AM1.5G). A reference cell based on a 2.5 μm titania film made of 20 nm sintered titania nanoparticles tested at the same conditions showed a lower performance, which is due to the significantly lower surface area of the titania layer prepared by the sintering approach.

dx.doi.org/10.1021/ja411292u | J. Am. Chem. Soc. 2014, 136, 5930–5937

CONCLUSIONS

In this study, we have demonstrated that novel porous titania thin film morphologies can be obtained by biotemplating with nanocrystalline cellulose (NCC). The main advantages of the NCC template compared to the traditionally used "soft templates", such as surfactant micelles include shape persistence, higher temperature stability, and tunable dimensions. The combination of these features permits tailoring the film morphology by varying the composition of the precursor mixture, the processing conditions, and post deposition treatments.

At a given NCC concentration, the concentration of the titania precursor is decisive for the resulting titania crystal size in the pore walls. To achieve the formation of a highly porous structure, the crystal size should be smaller than 12 nm. The surface area could be varied in the range from 61 to 175 m^2/g by adjusting the template content. In addition, significant pore expansion was achieved with a hydrothermal postsynthetic treatment, leading to a 2-fold increase in the total pore volume and an increase in the mean pore size from 9 to 13.5 nm.

To sum up, considerable changes in the surface area, pore size, and total pore volume can be realized with the same template by a moderate variation of the deposition conditions. We suggest that the pore formation in the NCC templated titania is mainly influenced by (i) the initial dimensions of cellulose rods, (ii) titania crystallization rate around the NCC rods, (iii) the NCC arrangement in the precursor solution and during the film coating, and (iv) the NCC thermal decomposition.

NCC templating offers the potential to supersede conventional approaches toward porous titania for diverse applications. The sustainable starting materials are widely available, and NCC-templated titania networks can be easily modified according to the requirements for the resulting materials or devices. Moreover, recent work in our laboratories shows that due to the unique properties of cellulose nanocrystals, this approach can also be extended to the fabrication of crystalline mesoporous thin films of other oxides.

EXPERIMENTAL SECTION

Synthesis. *NCC Preparation.* The cellulose crystals were extracted from Membrana cotton linters CP20 by sulfuric acid hydrolysis according to a modified procedure mentioned elsewhere.[29,54] A 300-mL portion of 64% H_2SO_4 was added to 34 g cotton. After 1 h, the mixture was heated to 55 °C for 30 min. The linters dissolved, and the solution became slightly yellow. Then the suspension was 10-fold diluted with deionized water. Afterward, it was left overnight to sediment the NCC-containing fraction. The upper liquid phase was decanted and the NCC-rich lower phase was washed three times with water via repeated centrifugation. Large cellulose aggregates were separated by centrifugation at 500 rpm, and the supernatant was collected. Finally, the suspension was concentrated in a rotary evaporator to 9−11 wt % at pH 1.7−2.3.

Precursor Preparation. Concentrated HCl was added to titanium(IV) ethoxide (TEOT), and the mixture was stirred approximately 10 min. After the full dissolution of TEOT, the required amounts of NCC suspension were introduced, and then water was added. The mixture was stirred for 2 h before the film deposition. The composition of precursor solutions is defined by the following parameters: titania to NCC mass ratio, Ti^{4+} concentration in mol/L, and NCC wt % concentration. TiO_2/NCC ratio 1.0 means that the NCC amount in grams was equal to the titania amount in grams calculated from the titanium ethoxide content in a precursor solution. Ti^{4+} concentration in mol/L was calculated, taking into account volumes of all liquid components of a precursor solution. NCC wt % concentration indicates the percentage of the NCC amount relative to the total precursor mass. For example, the precursor solution with a TiO_2/NCC ratio 0.75, 2.5 wt % NCC, and 0.23 mol/L Ti^{4+} was prepared according to the following recipe: 0.2143 g (0.9395 mmol) titanium(IV) ethoxide, 153 mg (1.846 mmol) 37% HCl, 1.155 g of 8.70 wt % NCC water suspension, and 2.49 mL H_2O.

Film Fabrication. The thin films for the SEM analysis were deposited on a 1.5 × 2.0 cm^2 silicon wafer by spin-coating 80 μL precursor solution at 2000 rmp for 40 s. X-ray diffraction, nitrogen sorption, and thermogravimetric analysis was performed on pulverized free-standing films. For their fabrication, the precursor solution was cast into a plastic Petri dish and dried at room temperature. Then the films were exposed to humidity or calcined directly. For the *delayed humidity treatment (DHT)*, the free-standing films were placed into a 2 L desiccator containing 80 mL KCl saturated solution and kept in an oven at 70 or 100 °C for 0.5−48 h. The films were calcined by using a stepwise 2 °C/min ramp with 2 h-steps of continuous heating at 100 °C, 360 °C, and a final step at 450 °C/30 min.

For the photocatalytic measurements and krypton sorption analysis, 250 μL precursor solution (TiO_2 g/NCC g = 0.75, 2.5 wt % NCC, 0.23 mol/L Ti^{4+}) was spin-coated on 2.5 × 2.5 cm^2 optical glass at 1500 rmp for 30 s, followed by 1 min film drying with a heat gun and N_2 flow. The spin-coating and drying were repeated 5 times. Then the film was calcined using 2 °C/min ramp with 2 h-steps of continuous heating at 100 °C, 360 °C, and final calcination at 500 °C/30 min. After the calcination, an additional 5 layers were deposited in a similar way and calcined at 500 °C/30 min. The weight of the 10-layered film coated on 2.5 × 2.5 cm^2 substrate was equal to 0.630 ± 0.05 mg.

For the photovoltaic measurements, the NCC-templated titania films were fabricated on 1.5 × 2.0 cm^2 FTO TEC-7 glass substrates coated with a dense titania blocking layer [100 μL solution of tetraethyl orthotitanate (0.525 mL), hydrochloric acid (37%, 0.375 mL) and tetrahydrofuran (7 mL) spin-coated at 4000 rmp for 40 s and calcined at 450 °C/30 min]. NCC containing precursor (TiO_2/NCC = 1.0 g/g, 2 wt % NCC, 0.28 mol/L Ti^{4+}) was dip-coated with 6 mm/s speed on top of the blocking layer. Then the films were placed in a 2 L desiccator containing 50 mL saturated KCl solution and kept in an oven at 70 °C/30 min with subsequent heating at 100 °C/30 min. The dip-coating and hydrothermal treatment steps were repeated four times. After the second and fourth layer, the films were calcined at 500 °C/30 min by using a 2 °C/min ramp with 2 h continuous heating steps at 100 and 360 °C, respectively. The anodes for the reference solar cells were obtained by diluting 0.281 g Dyesol 18 NRT paste in 0.45 mL ethanol and spin-coating 50 μL solution at 900 rmp on FTO glass with a blocking layer. The films were calcined at 500 °C for 30 min with a 11 h-ramp.

Solar Cell Assembly. Solar cells were prepared using a liquid iodine-based electrolyte, Pt-counter electrodes, and N719 dye according to the recipes and cell assemblage mentioned elsewhere.[55] The titania films were reduced (by removal from the surface) to an area of 0.55 × 0.55 cm^2, heated at 70 °C, and then immersed into a 0.5 mM solution of N719 dye in a mixture of acetonitrile and *tert*-butyl alcohol (1:1). After 16 h, the dye-coated electrodes were placed into acetonitrile for 1 h. Counter Pt-electrodes were prepared by depositing 10 μL of a 10 mM H_2PtCl_6 ethanol solution on a 1.5 × 2.0 cm^2 FTO substrate followed by heating at 450 °C for 15 min. The anode and the counter electrode were sealed on a hot plate by using a 25 μm Syrlin spacer. Then the "sandwich" was vacuum backfilled with the electrolyte through the predrilled hole in the Pt-electrode. The electrolyte solution contained 0.6 M butylmethylimidazolium iodide (BMII), 0.03 M iodine, 0.10 M guanidinium thiocyanate, and 0.50 M 4-*tert*butylpyridine in a mixture of acetonitrile and valeronitrile (85:15). Finally, the hole was sealed by 1.5 × 1.5 cm^2 Syrlin foil and a glass slide on top.

Characterization. Top views of porous titania films were analyzed using a JEOL JSM-6500F *scanning electron microscope (SEM)* equipped with a field emission gun, at 5 kV. Nanocrystalline cellulose SEM imaging was performed on a Verios XHR 460L microscope operating at 0.5 kV. High-resolution transmission electron microscopy (HRTEM) and scanning transmission electron microscopy in high-

dx.doi.org/10.1021/ja411292u | J. Am. Chem. Soc. 2014, 136, 5930−5937

angle annular dark field mode (STEM-HAADF) were performed using a FEI Titan 80−300 equipped with a field emission gun operated at 80 kV and 300 kV.

For the cellulose rod imaging, a water suspension of NCCs was dropped on holey-carbon coated copper grid and dried overnight. The *TEM analysis* was carried out at 80 kV. HRTEM of the film cross sections was performed at 300 kV by using STEM-HAADF mode. For the imaging of porous titania, we removed a thin film from a substrate or ground a free-standing film. Then the sample was dispersed in ethanol, and the solution was dropped on a holey-carbon coated copper grid. The imaging was performed at 300 kV.

X-ray diffraction analysis was carried out in reflection mode by using a Bruker D8 diffractometer with 1.5406 Å Ni-filtered Cu Kα radiation, operating at 40 kV and 40 mA. The mean crystallite size was calculated from broadening of the (101) anatase reflection by using the Scherrer equation.

The nitrogen sorption isotherms were obtained at −196 °C using a Quantachrome Autosorb-1. For the measurements 27 ± 3 mg of the sample was outgassed at 150 °C overnight. The specific surface area was determined with the Brunauer−Emmett−Teller (BET) method at p/p_0 = 0.05−0.2. The pore size distribution was determined with a DFT/Monte Carlo method and a NLDFT equilibrium model by using the Quantachrome Instruments Autosorb-1 software.

The krypton sorption isotherms at the boiling point of liquid nitrogen were obtained using an ASAP2010 (Micromeritics) apparatus. Three 2.5 × 2.5 cm^2 glass slides coated with porous titania film were simultaneously measured. Prior to the adsorption experiments, the sample was outgassed overnight at 200 °C. The saturation pressure of solid krypton of ca. 1.6 Torr and the cross-section of the krypton molecule of 0.21 nm^2 were used (as recommended by the producer of the equipment).

Thermogravimetric measurements were performed on a Netzsch STA 440 C TG/DSC with a heating rate of 1 °C/min in a stream of synthetic air of about 25 mL/min. UV−vis spectra were recorded with a Hitachi U-3501 spectrophotometer.

The experimental setup for the photocatalytic tests consisted of a gas supply part, the photoreactor, and a chemiluminiscent NO−NO_x gas analyzer. (Horiba ambient monitor APNA-360). The gaseous reaction mixture was prepared by mixing streams of dry air (1500 mL/min), wet air (1500 mL/min, relative humidity of 100%), and 50 ppm NO/N_2 (approximately 60 mL/min), in order to obtain a final concentration of NO of 1 ppm at a relative humidity of 50%. The photoreactor was illuminated by four 8 W black lights, the UV light intensity achieving 1 mW/cm^2. The size of the photocatalytic layer was 5 × 10 cm^2. Prior to the photocatalytic tests, the photoreactor was purged with the NO/water vapor/air mixture without illumination until a steady NO concentration was achieved at the outlet. It is readily calculated that 100% NO conversion would be equivalent to a photonic efficiency of ξ = 0.14%, assuming a mean irradiation wavelength of 350 nm.

4-Chlorophenol was photocatalytically degraded in a vessel 55 mL in volume, its initial concentration being 1 × 10^{-4} mol L^{-1}. The solution in the vessel was kept at 25 °C. Photocatalytic experiments were carried out without bubbling. The level of the liquid in the photoreactors was open to air under magnetic stirring, i.e., the concentration of dissolved oxygen was constant during the experiment owing to its equilibration with oxygen in the ambient air. A Sylvania Lynx-S 11 W BLB lamp irradiated the films with a UV light power reaching 1 mW cm^{-2} at the film surface. The irradiated area of the TiO_2 film was 12.5 cm^2. In each experiment, eight 0.5 mL aliquots were taken from the solution in the reaction vessel at regular time intervals and analyzed by HPLC.

The solar cells were illuminated at 100 mW/cm^2 with white light from an AM 1.5 G solar simulator (Solar Light Model 16S) equipped with a 150 W xenon lamp. The light intensity was adjusted by using a Fraunhofer ISE certified silicon reference cell.

■ ASSOCIATED CONTENT

Supporting Information

Electron micrographs of NCC and titania films, XRD patterns of NCC and titania films; photographs, UV−vis spectra and TGA data of NCC/titania films; sorption isotherms and porosity data of titania films; photocatalytic data. This material is available free of charge via the Internet at http://pubs.acs.org.

■ AUTHOR INFORMATION

Corresponding Author

bein@lmu.de

Notes

The authors declare no competing financial interest.

■ ACKNOWLEDGMENTS

This work was supported by the Nanosystems Initiative Munich excellence cluster funded by the German Research Foundation (DFG-NIM), the Bavarian SolTech research network, the German Academic Exchange Service (DAAD) and by the Academy of Sciences of the Czech Republic (Grant No. CZ12-DE02/2013-2014). The authors acknowledge Dr. Steffen Schmidt and Dr. Markus Döblinger for the TEM and SEM measurements; Dr. Florian Auras for the SEM analysis and Tina Reuther for the nitrogen sorption investigations. We thank FEI for the use of the Verios SEM. The authors thank the group of Prof. Peter Klüfers (LMU München) for providing cotton linters.

■ REFERENCES

(1) O'Regan, B.; Gratzel, M. *Nature* **1991**, *353*, 737−740.
(2) Szeifert, J. M.; Fattakhova-Rohlfing, D.; Georgiadou, D.; Kalousek, V.; Rathouský, J.; Kuang, D.; Wenger, S.; Zakeeruddin, S. M.; Grätzel, M.; Bein, T. *Chem. Mater.* **2009**, *21*, 1260−1265.
(3) Brinker, C. J.; Lu, Y.; Sellinger, A.; Fan, H. *Adv. Mater.* **1999**, *11*, 579−585.
(4) Soler-Illia, G. J. d. A. A.; Crepaldi, E. L.; Grosso, D.; Sanchez, C. *Curr. Opin. Colloid Interface Sci.* **2003**, *8*, 109−126.
(5) Lu, A. H.; Schüth, F. *Adv. Mater.* **2006**, *18*, 1793−1805.
(6) Lee, K.-R.; Kwon, Y.-U. *Nano* **2010**, *05*, 75−87.
(7) Sun, X.; Zheng, C.; Qiao, M.; Yan, J.; Wang, X.; Guan, N. *Chem. Commun.* **2009**, *31*, 4750−4752.
(8) He, W.; Cui, J.; Yue, Y.; Zhang, X.; Xia, X.; Liu, H.; Lui, S. *J. Colloid Interface Sci.* **2011**, *354*, 109−115.
(9) Han, T. H.; Oh, J. K.; Park, J. S.; Kwon, S.-H.; Kim, S.-W.; Kim, S. O. *J. Mater. Chem.* **2009**, *19*, 3512−3516.
(10) Yang, F.; Ma, Y.; Zhou, Y.; Pei, C.; Luo, Q.; Zeng, M.; Dai, B. *Curr. Nanosci.* **2011**, *7*, 1004−1008.
(11) Jeffryes, C.; Campbell, J.; Li, H.; Jiao, J.; Rorrer, G. *Energy Environ. Sci.* **2011**, *4*, 3930−3941.
(12) Shi, N.; Li, X.; Fan, T.; Zhou, H.; Ding, J.; Zhang, D.; Zhu, H. *Energy Environ. Sci.* **2011**, *4*, 172−180.
(13) Jia, Y.; Han, W.; Xiong, G.; Yang, W. *J. Colloid Interface Sci.* **2008**, *323*, 326−331.
(14) Losic, D.; Triani, G.; Evans, P. J.; Atanacio, A.; Mitchell, J. G.; Voelcker, N. H. *J. Mater. Chem.* **2006**, *16*, 4029−4034.
(15) Chen, J.; Su, H.; Song, F.; Moon, W.-J.; Kim, Y.-S.; Zhang, D. *J. Colloid Interface Sci.* **2012**, *370*, 117−123.
(16) Galusha, J. W.; Jorgensen, M. R.; Bartl, M. H. *Adv. Mater.* **2010**, *22*, 107−110.
(17) Sachse, A.; Hulea, V.; Kostov, K. L.; Marcotte, N.; Boltoeva, M. Y.; Belamie, E.; Alonso, B. *Chem. Commun.* **2012**, *48*, 10648−10650.
(18) Kimling, M. C.; Caruso, R. A. *J. Mater. Chem.* **2012**, *22*, 4073−4082.

(19) Zollfrank, C.; Cromme, P.; Rauch, M.; Scheel, H.; Kostova, M. H.; Gutbrod, K.; Gruber, S.; Van Opdenbosch, D. *Bioinsp. Biomim. Nanobiomater.* **2012**, *1*, 13−25.
(20) Lin, N.; Huang, J.; Dufresne, A. *Nanoscale* **2012**, *4*, 3274−3294.
(21) Tingaut, P.; Zimmermann, T.; Sebe, G. *J. Mater. Chem.* **2012**, *22*, 20105−20111.
(22) Gu, Y.; Huang, J. *J. Mater. Chem.* **2009**, *19*, 3764−3770.
(23) Pääkkö, M.; Ankerfors, M.; Kosonen, H.; Nykänen, A.; Ahola, S.; Österberg, M.; Ruokolainen, J.; Laine, J.; Larsson, P. T.; Ikkala, O.; Lindström, T. *Biomacromolecules* **2007**, *8*, 1934−1941.
(24) Isogai, A.; Saito, T.; Fukuzumi, H. *Nanoscale* **2011**, *3*, 71−85.
(25) Klemm, D.; Kramer, F.; Moritz, S.; Lindström, T.; Ankerfors, M.; Gray, D.; Dorris, A. *Angew. Chem., Int. Ed.* **2011**, *50*, 5438−5466.
(26) Revol, J. F.; Bradford, H.; Giasson, J.; Marchessault, R. H.; Gray, D. G. *Int. J. Biol. Macromol.* **1992**, *14*, 170−172.
(27) Dujardin, E.; Blaseby, M.; Mann, S. *J. Mater. Chem.* **2003**, *13*, 696−699.
(28) Thomas, A.; Antonietti, M. *Adv. Funct. Mater.* **2003**, *13*, 763−766.
(29) Shopsowitz, K. E.; Qi, H.; Hamad, W. Y.; MacLachlan, M. J. *Nature* **2010**, *468*, 422−425.
(30) Shopsowitz, K. E.; Hamad, W. Y.; MacLachlan, M. J. *Angew. Chem., Int. Ed.* **2011**, *50*, 10991−10995.
(31) Shopsowitz, K. E.; Hamad, W. Y.; MacLachlan, M. J. *J. Am. Chem. Soc.* **2011**, *134*, 867−870.
(32) Shopsowitz, K. E.; Stahl, A.; Hamad, W. Y.; MacLachlan, M. J. *Angew. Chem., Int. Ed.* **2012**, *51*, 6886−6890.
(33) Kettunen, M.; Silvennoinen, R. J.; Houbenov, N.; Nykänen, A.; Ruokolainen, J.; Sainio, J.; Pore, V.; Kemell, M.; Ankerfors, M.; Lindström, T.; Ritala, M.; Ras, R. H. A.; Ikkala, O. *Adv. Funct. Mater.* **2011**, *21*, 510−517.
(34) Korhonen, J. T.; Hiekkataipale, P.; Malm, J.; Karppinen, M.; Ikkala, O.; Ras, R. H. A. *ACS Nano* **2011**, *5*, 1967−1974.
(35) Zhang, D.; Qi, L. *Chem. Commun.* **2005**, 2735−2737.
(36) Chen, X.-Y; Chen, X.; Hong, S.-W.; Chen, X.; Huang, B. *Chin. J. Catal.* **2011**, *32*, 1762−1767.
(37) Liu, X.; Gu, Y.; Huang, J. *Chem.—Eur. J.* **2010**, *16*, 7730−7740.
(38) Li, X.; Fan, T.; Zhou, H.; Chow, S.-K.; Zhang, W.; Zhang, D.; Guo, Q.; Ogawa, H. *Adv. Funct. Mater.* **2009**, *19*, 45−56.
(39) Ghadiri, E.; Taghavinia, N.; Zakeeruddin, S. M.; Grätzel, M.; Moser, J.-E. *Nano Lett.* **2010**, *10*, 1632−1638.
(40) Lee, Y. M.; Kim, Y. H.; Lee, J. H.; Park, J. H.; Park, N.-G.; Choe, W.-S.; Ko, M. J.; Yoo, P. J. *Adv. Funct. Mater.* **2011**, *21*, 1160−1167.
(41) Alonso, B.; Belamie, E. *Angew. Chem., Int. Ed.* **2010**, *49*, 8201−8204.
(42) Belamie, E.; Boltoeva, M. Y.; Yang, K.; Cacciaguerra, T.; Alonso, B. *J. Mater. Chem.* **2011**, *21*, 16997−17006.
(43) Shao, S.; Dimitrov, M.; Guan, N.; Kohn, R. *J. Mater. Chem.* **2009**, *19*, 8411−8417.
(44) Li, X.; Birnbaum, J. C.; Williford, R. E.; Fryxell, G. E.; Coyle, C. A.; Dunham, G. C.; Baskaran, S. *Chem. Commun.* **2003**, *20*, 2054−2055.
(45) Crepaldi, E. L.; Soler-Illia, G. J. d. A. A.; Grosso, D.; Cagnol, F.; Ribot, F.; Sanchez, C. *J. Am. Chem. Soc.* **2003**, *125*, 9770−9786.
(46) Fulvio, P. F.; Grabicka, B. E.; Grudzien, R. M.; Jaroniec, M. *Adsorpt. Sci. Technol.* **2007**, *25*, 439−449.
(47) Morishige, K.; Tateishi, M.; Hirose, F.; Aramaki, K. *Langmuir* **2006**, *22*, 9220−9224.
(48) Cao, L.; Man, T.; Kruk, M. *Chem. Mater.* **2009**, *21*, 1144−1153.
(49) Sayari, A.; Kruk, M.; Jaroniec, M.; Moudrakovski, I. L. *Adv. Mater.* **1998**, *10*, 1376−1379.
(50) Aulin, C.; Ahola, S.; Josefsson, P.; Nishino, T.; Hirose, Y.; Österberg, M.; Wågberg, L. *Langmuir* **2009**, *25*, 7675−7685.
(51) Szeifert, J. M.; Fattakhova-Rohlfing, D.; Rathouský, J.; Bein, T. *Chem. Mater.* **2012**, *24*, 659−663.
(52) Procházka, J.; Kavan, L.; Shklover, V.; Zukalová, M. t.; Frank, O.; Kalbáč, M.; Zukal, A. t.; Pelouchová, H.; Janda, P.; Mocek, K.; Klementová, M.; Carbone, D. *Chem. Mater.* **2008**, *20*, 2985−2993.
(53) Rathousky, J.; Kalousek, V.; Kolar, M.; Jirkovsky, J. *Photochem. Photobiol. Sci.* **2011**, *10*, 419−424.
(54) Dong, X. M.; Kimura, T.; Revol, J.-F.; Gray, D. G. *Langmuir* **1996**, *12*, 2076−2082.
(55) Ito, S.; Murakami, T. N.; Comte, P.; Liska, P.; Grätzel, C.; Nazeeruddin, M. K.; Grätzel, M. *Thin Solid Films* **2008**, *516*, 4613−4619.